






RESEARCH ARTICLE | FEBRUARY 02 2024

## Analysis of a Reiner–Rivlin liquid sphere enveloped by a permeable layer **FREE**

R. Selvi (आर सेल्वी) ; Deepak Kumar Maurya (दीपक कुमार मौर्य)  ; Pankaj Shukla (पंकज शुक्ला) ;  
Ali J. Chamkha (أ. ج. شامخا) 



*Physics of Fluids* 36, 023303 (2024)

<https://doi.org/10.1063/5.0182706>



View  
Online



Export  
Citation

CrossMark



**Physics of Fluids**  
Special Topic:  
Flow and Civil Structures

**Submit Today**



# Analysis of a Reiner–Rivlin liquid sphere enveloped by a permeable layer

Cite as: Phys. Fluids **36**, 023303 (2024); doi: [10.1063/5.0182706](https://doi.org/10.1063/5.0182706)

Submitted: 20 October 2023 · Accepted: 6 January 2024 ·

Published Online: 2 February 2024



View Online



Export Citation



CrossMark

R. Selvi (आर० सेल्वी०),<sup>1,a)</sup> Deepak Kumar Maurya (दीपक कुमार मौर्य),<sup>2,b)</sup> Pankaj Shukla (पंकज शुक्ला),<sup>3,c)</sup> and Ali J. Chamkha (علي ج. شامخة),<sup>4,d)</sup>

## AFFILIATIONS

<sup>1</sup>Department of Mathematics, The Institute of Mathematical Sciences, Chennai 600113, Tamil Nadu, India

<sup>2</sup>Department of Mathematics, Prof. Rajendra Singh (Rajju Bhaiya) Institute of Physical Sciences for Study and Research, Veer Bahadur Singh Purvanchal University, Jaunpur 222003, Uttar Pradesh, India

<sup>3</sup>Department of Mathematics, VIT University, Chennai 600127, Tamil Nadu, India

<sup>4</sup>Faculty of Engineering, Kuwait College of Science and Technology, Doha 35004, Kuwait

<sup>a)</sup>Electronic mail: [selviaiva@gmail.com](mailto:selviaiva@gmail.com)

<sup>b)</sup>Author to whom correspondence should be addressed: [deepak893395@gmail.com](mailto:deepak893395@gmail.com)

<sup>c)</sup>Electronic mail: [pankaj.shukla@vit.ac.in](mailto:pankaj.shukla@vit.ac.in)

<sup>d)</sup>Electronic mail: [a.chamkha@kcst.edu.kw](mailto:a.chamkha@kcst.edu.kw)

## ABSTRACT

The present article investigates the axisymmetric flow of a steady incompressible Reiner–Rivlin liquid sphere enveloped by a spherical porous layer using the cell model technique. The Brinkman-extended Darcy model is deployed for the porous medium hydrodynamics, and isotropic permeability is considered. The stream function solutions of the governing equations are obtained, which involves the Gegenbauer functions and the modified Bessel functions. An asymptotic series expansion in terms of the Reiner–Rivlin liquid parameter  $S$  has been employed to determine the expression of the flow field for the Reiner–Rivlin liquid. Boundary conditions on the cell surface corresponding to the Happel, Kuwabara, Kvashnin, and Cunningham models are considered. Analytical expressions are derived for dimensionless pressure, tangential stress, and the couple stress components using the method of separation of variables and Gegenbauer functions/polynomial. The integration constants are evaluated with appropriate boundary conditions on the inner and outer boundary of the porous zone with the aid of Mathematica symbolic software. Solutions for the drag force exerted by the Reiner–Rivlin fluid on the porous sphere are derived with corresponding expressions for the drag coefficient. Mathematical expression of the drag coefficient, pressure distribution, velocity profile, and separation parameter is established. On the basis of viscosity ratio, permeability parameter, dimensionless parameter, and the volume fraction, variations of the drag coefficient, velocity profiles, fluid pressure, and separation parameter (SEP) are investigated with their plots. The effects of the streamline pattern make the flow more significant for the Mehta–Morse when compared to the other models. Additionally, the mathematical expression of the separation parameter (SEP) is also calculated, which shows that no flow separation occurs for the considered flow configuration and is also validated by its pictorial depiction. This problem is motivated by emulsion hydrodynamics in chemical engineering where rheological behavior often arises in addition to porous media effects.

Published under an exclusive license by AIP Publishing. <https://doi.org/10.1063/5.0182706>

## NOMENCLATURE

$a$	Radius of Reiner–Rivlin liquid sphere	$k$	Permeability of saturated porous sphere
$b$	Radius of hypothetical cell	$p$	Fluid pressure
$D_N$	Drag coefficient	$(r, \theta, \phi)$	Spherical coordinates
$d_{ij}$	Rate of deformation tensor	$S$	Reiner–Rivlin liquid parameter
$(\hat{e}_r, \hat{e}_\theta)$	Unit vectors	$(v_r, v_\theta)$	Velocity components
$F$	Drag force	$\gamma$	Volume fraction
$G_2(\zeta)$	Gegenbauer functions	$\delta$	Thickness of porous layer
		$\delta_{ij}$	Kronecker delta
		$\mu_1$	Viscosity of Newtonian fluid

$\mu_2$	Viscosity of Reiner–Rivlin liquid
$\mu_c$	Cross-viscosity for region II
$\mu_e$	Effective viscosity due to porous medium
$\tau_{ij}$	Stress tensor
$\psi$	Stream function

## I. INTRODUCTION

A substance having pores, or voids, is referred to as a porous medium or porous material.<sup>1</sup> The momentum equation and the equation of continuity work together to control the flow in porous media.<sup>2</sup> The Brinkman equation<sup>3</sup> is an equation, which is created by adding the viscous term to the Darcy equation<sup>4</sup> or removing the inertial term from the Navier–Stokes equation.<sup>5</sup> Within the scope of micropolar and Newtonian fluid models, the characteristics of nanocapillary flows are investigated by Khanukaeva and Troshkin.<sup>6</sup> The cell model technique is an effective tool to investigate the flow in permeable media through concentrated dispersion and membranes.<sup>7</sup> The idea behind the cell model technique involves assembling random groups of particles that can be separated into numerous identical cells. In the case of spheres, the fundamental idea of the cell model indicates that a system of randomly oriented spherical particles is replaced by a periodic array of spheres contained in identical spherical liquid cells. The boundary conditions on the hypothetical cell surface are considered to be taken into account under the impact of surrounding particles at the cell's core. In the cell models, proposed by Happel,<sup>8</sup> Kuwabara,<sup>9</sup> Kvashnin,<sup>10</sup> and Mehta–Morse,<sup>11</sup> both particle and outer hypothetical cell are identical spheres/cylinders. In the Happel model, no shearing stress on the cell surface is applied, while nil vorticity condition is applied on the cell surface in the Kuwabara model. The Kvashnin model assumes that the tangential component velocity reaches a minimum with respect to the radial coordinate, thereby the symmetry on the cell is signified. The Mehta–Morse model assumed that the “homogeneity of the flow on the cell boundary” signifies the tangential velocity as a component of the average fluid velocity.

In cylindrical coordinates, the constitutive formulations<sup>12</sup> of a Reiner–Rivlin liquid are produced by taking into consideration the Reiner–Rivlin model in combination with the implications of an unvarying axial magnetic strength. Deo *et al.*<sup>13</sup> investigated the hydrodynamic permeability of membranes composed of porous spherical particles with an impermeable core utilizing the cell model. Saad<sup>14</sup> reported the analytical solution for the problem of an incompressible non-Newtonian fluid through a viscous fluid sphere using the terminology of cell methods. Jaiswal and Gupta<sup>15</sup> investigated the problem of creeping flow past a swarm of Reiner–Rivlin fluid spherical drops using the cell model. Selvi and Shukla<sup>16</sup> researched the creeping fluid through a non-Newtonian fluid-saturated porous medium with no spin condition. Selvi and Shukla<sup>17</sup> studied the Stokes fluid past a micropolar fluid with a saturated porous medium using cell model with zero spin condition. Selvi *et al.*<sup>18</sup> concluded that the micropolar fluid sphere is larger than the permeable region, in the study of micropolar fluid around the spherical drops of non-Newtonian fluid surrounded by a permeable layer. The drag force of a spherical bubble in a Newtonian fluid containing a Reiner–Rivlin fluid contaminated with a monomolecular layer of surfactant film was previously estimated by Raturi and Kumar.<sup>19</sup> Jaiswal<sup>20</sup> investigated the steady Stokes axisymmetrical Reiner–Rivlin streaming flow over a fixed viscous droplet with a sphere-like deformation in its shape. Selvi *et al.*<sup>21</sup> investigated

the encapsulated drops in a Newtonian fluid with the effect of no-slip condition. Using four existing cell models, Deo *et al.*<sup>22</sup> investigated the influence of an external magnetic field on the hydrodynamic permeability of a biporous membrane relative to the motion of a micropolar liquid. Selvi and Shukla<sup>23</sup> explored the special condition of the Mehta–Morse model in the motion of fluid flow in a Reiner–Rivlin liquid covered by micropolar fluid.

Microalgae and bacteria have a higher density than water, which causes them to go upward and against gravity. This phenomenon<sup>24</sup> causes the top layer to thicken more than the bottom layer, which throws the density distribution out of balance. Selvi<sup>25</sup> researched the semipermeable region within the couple stress fluid sphere. They concluded that tangential stress increases in the semipermeable region with increasing the couple stress fluid. Deo and Maurya<sup>26</sup> explored the influence of a magnetic field on the flow of a Newtonian fluid sandwiched between two non-Newtonian fluid layers through a rectangular porous channel. Maurya and Deo<sup>27</sup> deals with the influence of magnetic field on Newtonian fluid sandwiched between two porous cylindrical pipes, which are filled with micropolar fluids. Maurya *et al.*<sup>28</sup> investigated the Stokes flow of a non-Newtonian fluid through a porous cylinder whose axis is perpendicular to the direction of fluid flow. A uniform magnetic field acting perpendicular to the axis of two concentric rotating cylinders and moving parallel to it, as well as an unsteady flow of an incompressible Reiner–Rivlin liquid around the common axis of these cylinders, was described by Deo and Kumar.<sup>29</sup> Ramkissoon<sup>30</sup> examined the problem of axisymmetrical flow of a Newtonian fluid past a Reiner–Rivlin liquid sphere. In the presence of a uniform magnetic field, Maurya *et al.*<sup>31</sup> investigated the Stokesian flow of an axisymmetric, incompressible couple stress fluid through a porous material surrounding a solid sphere. Recently, Selvi *et al.*<sup>32</sup> studied the flow of an incompressible couple stress fluid through a Reiner–Rivlin liquid surrounded by a permeable medium.

Using the cell model technique, the proposed article studies the axisymmetric flow of a steady incompressible Reiner–Rivlin liquid sphere enclosed by a spherical porous layer. For the flow outside the liquid sphere layer, the Brinkman equation is employed. The stream function solutions to the governing equations, which include the Gegenbauer functions and modified Bessel functions, are derived. The formulation of the flow field for the Reiner–Rivlin liquid was determined using an asymptotic series expansion in terms of the Reiner–Rivlin liquid parameter  $S$ . The boundary conditions of the Happel, Kuwabara, Kvashnin, and Mehta–Morse models are used on the cell surface. The drag coefficient, pressure distribution, velocity profile, and separation parameter are all mathematically expressed. Variations of the drag coefficient, velocity profiles, fluid pressure, and separation parameter (SEP) are explored using plots based on the viscosity ratio, permeability parameter, dimensionless parameter, and volume fraction. When compared to the other models, the effects of the streamline pattern make the flow more relevant for the Mehta–Morse, and it is also worth noting that no flow separation occurs for an existing flow configuration.

## II. MATHEMATICAL FORMULATION

In the present research idea, we have investigated a mathematical model connecting the flow of the Reiner–Rivlin liquid occupied within a sphere of radius “ $a$ ,” which is enveloped by a hypothetical spherical porous cell of radius “ $b$ ” (Fig. 1). The cell region is filled by a Newtonian fluid, and the porous medium is taken as homogeneous

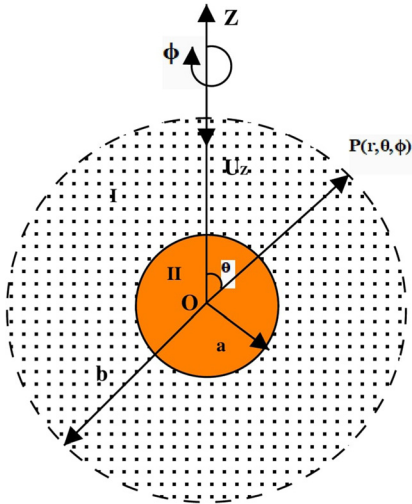


FIG. 1. Physical representation of the problem.

and isotropic. The radius  $b$  of hypothetical cell is determined in such a way that the volume fraction of the cell equals the particle volume fraction  $\gamma$  of the porous cylinder coated with another porous layer. Mathematically,

$$\gamma = \frac{\text{Volume of inner sphere } (4\pi a^2)}{\text{Volume of hypothetical sphere } (4\pi b^2)}. \quad (1)$$

For our convenience, we are introducing two parameters: one is  $l$  and the other is  $\delta$ , and these are defined as follows:

$$\gamma = \frac{1}{l^2} \quad \text{and} \quad \delta = 1 - l \Rightarrow l = \frac{b}{a} \quad \text{and} \quad \delta = \frac{a - b}{a}. \quad (2)$$

The flow pattern is taken as steady, axisymmetric, and incompressible by neglecting the body force and body couple. The flow regime is separated into region I and region II in which region I stands for hypothetical cell region, i.e.,  $a \leq r \leq b$  and region II, i.e.,  $0 \leq r \leq a$  represents for inner spherical region filled with the Reiner-Rivlin liquid. Defining a new parameter  $\alpha$  connecting the viscosities  $\mu_1$  and  $\mu_e$  and permeability  $k$  as follows:

$$\alpha^2 = \frac{b^2 \mu_1}{k \mu_e}.$$

For the region I, the governing equations are given by

$$\nabla \cdot \vec{v}^{(1)} = 0, \quad (3)$$

$$\nabla^2 \vec{v}^{(1)} - \left(\frac{\alpha}{b}\right)^2 \vec{v}^{(1)} = \frac{1}{\mu_e} \nabla p^{(1)}. \quad (4)$$

The governing equations for region II are given by the constitutive equation of isotropic Reiner-Rivlin liquids as

$$\tau_{ij} = -p^{(2)} \delta_{ij} + 2\mu_2 d_{ij} + \mu_c d_{ik} d_{kj}, \quad (5)$$

where  $d_{ij} = \frac{1}{2}(v_{ij}^{(2)} + v_{ji}^{(2)})$  and comma (,) represents the partial derivative.

Since the flow field is in the meridian plane and the flow is axisymmetric, therefore the flow field will be independent of coordinate  $\phi$ . In such type of circumstances, fluid velocity vector can be taken as

$$\vec{v}^{(i)} = v_r^{(i)}(r, \theta) \hat{e}_r + v_\theta^{(i)}(r, \theta) \hat{e}_\theta. \quad (6)$$

To satisfy the equation of continuity, we can introduce a scalar valued function  $\psi^{(i)}(r, \theta)$ , named by stream function as follows:

$$v_r^{(i)} = -\frac{1}{r^2 \sin \theta} \frac{\partial \psi^{(i)}}{\partial \theta} \quad \text{and} \quad v_\theta^{(i)} = \frac{1}{r \sin \theta} \frac{\partial \psi^{(i)}}{\partial r}. \quad (7)$$

Using the curl operator, eliminating the pressure from the Eq. (4) with the help of Eq. (7), we get

$$E^2(E^2 - \alpha^2)\psi^{(1)} = 0, \quad (8)$$

where  $E^2 = \frac{\partial}{\partial r^2} + \frac{\sin \theta}{r^2} \frac{\partial}{\partial \theta} \left( \frac{1}{\sin \theta} \frac{\partial}{\partial \theta} \right)$ .

Introducing two functions  $y_{-2}(ar)$  and  $y_2(ar)$ , which are the combination of modified Bessel functions  $I_{\frac{3}{2}}(ar)$  and  $K_{\frac{3}{2}}(ar)$  and are given by expressions,

$$\begin{aligned} y_{-2}(ar) &= \alpha \cosh(ar) - \frac{1}{r} \sinh(ar), \\ y_2(ar) &= \alpha \sinh(ar) - \frac{1}{r} \cosh(ar). \end{aligned} \quad (9)$$

Therefore, the stream function solution of Eq. (8) can be expressed as follows:

$$\begin{aligned} \psi^{(1)}(r, \zeta) &= \left[ A_1 r^2 + \frac{B_1}{r} + C_1 y_{-2}(ar) + D_1 y_2(ar) \right] G_2(\zeta), \\ G_2(\zeta) &= \frac{(1 - \zeta^2)}{2}, \end{aligned} \quad (10)$$

where  $A_1, B_1, C_1$ , and  $D_1$  are arbitrary constants and  $G_2(\zeta)$  is the Gegenbauer polynomial with  $\zeta = \cos \theta$ .

Analytical solutions for the stream function and pressure within the liquid core (Reiner-Rivlin droplet) are challenging to determine. However, asymptotic solutions for these fluid quantities can be easily investigated. To determine the asymptotic solutions<sup>30</sup> for the stream function and the pressure, the power series expansions in terms of the Reiner-Rivlin parameter  $S$ , which is very small, are introduced in the following form:

$$\psi^{(2)} = \psi_0 + \psi_1 S + \psi_2 S^2 + \dots \quad \text{and} \quad p^{(2)} = p_0 + p_1 S + p_2 S^2 + \dots, \quad (11)$$

where  $S = \frac{\mu_c U}{\mu_2 a}$ ,  $E^4 \psi_0 = 0$ ,  $E^4 \psi_1 = 8r \sin^2 \theta \cos \theta$ , and

$$E^4 \psi_2 = \frac{32}{3} r^2 \sin^2 \theta. \quad (12)$$

Asymptotic solutions of Eq. (12) can be represented as

$$\begin{aligned} \psi_0 &= (r^4 - r^2) \sin^2 \theta, \quad \psi_1 = \frac{2}{21} r^5 \sin^2 \theta \cos \theta, \\ \text{and} \quad \psi_2 &= \frac{2}{63} r^6 \sin^2 \theta. \end{aligned} \quad (13)$$

So, the stream function can be expressed as follows:

$$\psi^{(2)}(r, \zeta) = \psi_0 + \psi_1 S + \psi_2 S^2 + \sum_{n=2}^{\infty} [a_n r^n + b_n r^{n+2}] G_n(\zeta), \quad (14)$$

where  $a_n$  and  $b_n$ ,  $n = 2, 3, \dots$  are unknown parameters.

After substituting of the expressions of stream functions  $\psi_0, \psi_1, \psi_2$  into Eq. (14), we have obtained the explicit expression of stream function  $\psi_2$  in terms of the Gegenbauer polynomial, and it is

$$\begin{aligned} \psi^{(2)}(r, \zeta) = & \left[ (a_2 - 2)r^2 + (b_2 + 2)r^4 + \frac{4}{63}S^2r^6 \right] G_2(\zeta) \\ & + \left[ a_3r^3 + \left( b_3 + \frac{4}{21}S \right) r^5 \right] G_3(\zeta) \\ & + \sum_{n=4}^{\infty} [a_n r^n + b_n r^{n+2}] G_n(\zeta). \end{aligned} \quad (15)$$

### III. BOUNDARY CONDITIONS

In order to find out the arbitrary constants  $A_1, B_1, C_1, D_1, a_2, b_2$ , suitable boundary conditions are applied on the inner and outer cell surfaces. The unknown constants involved in the Eqs. (10) and (15) are determined using the following boundary conditions.

#### A. Conditions on the inner surface at $r = a$

$$\text{Impenetrability condition} \Rightarrow \psi_{\theta}^{(i)} = 0, \quad i = 1, 2. \quad (16)$$

$$\text{Continuity of tangential velocity} \Rightarrow \psi_r^{(1)} = \psi_r^{(2)}. \quad (17)$$

$$\begin{aligned} \text{Continuity of the tangential stress} \Rightarrow \mu_1 \frac{\partial}{\partial r} \left( \frac{1}{r^2} \frac{\partial \psi^{(1)}}{\partial r} \right) \\ = \mu_2 \frac{\partial}{\partial r} \left( \frac{1}{r^2} \frac{\partial \psi^{(2)}}{\partial r} \right). \end{aligned} \quad (18)$$

#### B. Conditions on the hypothetical cell surface at $r = l$

The proposed cell models by Happel, Kuwabara, Kvashnin, and Mehta–Morse require the following condition at the cell surface:

$$v_r^{(1)} = \cos \theta, \quad \text{i.e.,} \quad \frac{\partial \psi^{(1)}}{\partial \theta} = r^2 \sin \theta \cos \theta. \quad (19)$$

- (i) The Happel model<sup>8</sup> implies that the condition of tangential stress vanishes on the cell surface,

$$\tau_{r\theta}^{(1)} = 0, \quad \text{i.e.,} \quad \frac{-\cot \theta \partial \psi^{(1)}}{r^2 \partial \theta} + \frac{1}{r^2} \frac{\partial^2 \psi^{(1)}}{\partial \theta^2} - \frac{\partial^2 \psi^{(1)}}{\partial r^2} - \frac{2}{r} \frac{\partial \psi^{(1)}}{\partial r} = 0. \quad (20)$$

- (ii) The Kuwabara model<sup>9</sup> assumes that the curl of velocity on the cell surface vanishes and the flow is assumed to be a potential one,

$$\nabla \times \vec{v} = \vec{0}, \quad \text{i.e.,} \quad \frac{\cot \theta \partial \psi^{(1)}}{r^2 \partial \theta} - \frac{1}{r^2} \frac{\partial^2 \psi^{(1)}}{\partial \theta^2} - \frac{\partial^2 \psi^{(1)}}{\partial r^2} = 0. \quad (21)$$

- (iii) The Kvashnin model<sup>10</sup> suggests the cell symmetry condition on the cell surface,

$$\frac{\partial v_{\theta}^{(1)}}{\partial r} = 0, \quad \text{i.e.,} \quad \frac{1}{r} \frac{\partial \psi^{(1)}}{\partial r} - \frac{\partial^2 \psi^{(1)}}{\partial r^2} = 0. \quad (22)$$

- (iv) The Mehta–Morse model<sup>11</sup> assumes the homogeneity, i.e., uniform velocity condition, on the cell surface,

$$v_{\theta}^{(1)} = -\sin \theta, \quad \text{i.e.,} \quad \frac{\partial \psi^{(1)}}{\partial r} = r \sin^2 \theta. \quad (23)$$

### IV. DETERMINATION OF ARBITRARY PARAMETERS

Employing the boundary conditions (16)–(23) into Eqs. (10) and (15), we get the following algebraic linear equations:

$$A_1 + B_1 + C_1 y_{-2}(\alpha) + D_1 y_2(\alpha) = 0, \quad (24)$$

$$a_2 + b_2 = \frac{-4}{63} S^2, \quad (25)$$

$$\begin{aligned} 2A_1 - B_1 + C_1 [\alpha^2 y_{-1}(\alpha) - y_{-2}(\alpha)] + D_1 [\alpha^2 y_1(\alpha) - y_2(\alpha)] \\ = 4 + \frac{8S^2}{21} + 2a_2 + 4b_2, \end{aligned} \quad (26)$$

$$\begin{aligned} -2A_1 \lambda^2 + 4B_1 \lambda^2 + C_1 [\alpha^2 \lambda^2 y_{-2}(\alpha) + 4\lambda^2 y_{-2}(\alpha) - 2\alpha^2 \lambda^2 y_{-1}(\alpha)] \\ + D_1 [\alpha^2 \lambda^2 y_2(\alpha) + 4\lambda^2 y_2(\alpha) - 2\alpha^2 \lambda^2 y_1(\alpha)] = 12 + \frac{8S^2}{7} - 2a_2 + 4b_2, \end{aligned} \quad (27)$$

$$A_1 l^2 + B_1 l^{-1} + C_1 y_{-2}(\alpha l) + D_1 y_2(\alpha l) = l^2. \quad (28)$$

#### A. For Happel's model

$$\begin{aligned} 6l^{-3} B_1 + C_1 [\alpha^2 y_{-2}(\alpha l) + 6l^{-2} y_{-2}(\alpha l) - 2\alpha^2 l^{-1} y_{-1}(\alpha l)] \\ + D_1 [\alpha^2 y_2(\alpha l) + 6l^{-2} y_2(\alpha l) - 2\alpha^2 l^{-1} y_1(\alpha l)] = 0. \end{aligned} \quad (29)$$

Systems of linear equations (24)–(29) are solved for values of unknown parameters  $A_1, B_1, C_1, D_1, a_2, b_2$ .

#### B. For Kuwabara's model

$$C_1 y_{-2}(\alpha l) + D_1 y_2(\alpha l) = 0. \quad (30)$$

Systems of linear equations from Eqs. (24)–(28) with Eq. (30) are solved for  $A_1, B_1, C_1, D_1, a_2, b_2$ .

#### C. For Kvashnin's model

$$\begin{aligned} 3l^{-3} B_1 + C_1 [\alpha^2 y_{-2}(\alpha l) + 3l^{-2} y_{-2}(\alpha l) - \alpha^2 l^{-1} y_{-1}(\alpha l)] \\ + D_1 [\alpha^2 y_2(\alpha l) + 3l^{-2} y_2(\alpha l) - \alpha^2 l^{-1} y_1(\alpha l)] = 0. \end{aligned} \quad (31)$$

Systems of linear equations using Eqs. (24)–(28) together with Eq. (31) are solved for unknowns  $A_1, B_1, C_1, D_1, a_2, b_2$ .

#### D. For Mehta–Morse's model

$$\begin{aligned} 2A_1 l - l^{-2} B_1 + C_1 [-l^{-1} y_{-2}(\alpha l) + \alpha^2 y_{-1}(\alpha l)] \\ + D_1 [-l^{-1} y_2(\alpha l) + \alpha^2 y_1(\alpha l)] = 0. \end{aligned} \quad (32)$$

Systems of linear equations from Eqs. (24)–(28) with Eq. (32) are solved using MATHEMATICA software for unique values of  $A_1, B_1, C_1, D_1, a_2, b_2$ .

V. EXPRESSION OF STREAM FUNCTION

Determined constant values for each case are very burdensome; therefore, their expressions are not mentioned in the manuscript. Hence, the non-dimensional stream functions for the regions I and II are given, respectively, by

$$\begin{aligned} \psi^{(1)}(r, \zeta) &= \left[ A_1 r^2 + \frac{B_1}{r} + C_1 y_{-2}(\alpha r) + D_1 y_2(\alpha r) \right] G_2(\zeta), \quad 1 \leq r \leq \gamma^{-1}, \\ \psi^{(2)}(r, \zeta) &= \left[ (a_2 - 2)r^2 + (b_2 + 2)r^4 + \frac{4}{63} S^2 r^6 \right] G_2(\zeta) \\ &+ \left[ a_3 r^3 + \left( b_3 + \frac{4}{21} S \right) r^5 \right] G_3(\zeta) \\ &+ \sum_{n=4}^{\infty} \left[ a_n r^n + b_n r^{n+2} \right] G_n(\zeta), \quad r \leq 1. \end{aligned} \tag{33}$$

VI. CALCULATION OF THE DRAG FORCE

The drag force  $F$  exerted on a permeable sphere is estimated using the following formula:<sup>33</sup>

$$F = 4\pi\mu_1 U a \alpha^2 \lim_{r \rightarrow \infty} r^3 \left[ \frac{\psi^{(1)} - \psi_{\infty}^{(1)}}{\tilde{\omega}^2} \right], \quad \text{where } \tilde{\omega} = r \sin \theta. \tag{34}$$

$$\Rightarrow F = 2\pi\mu_1 U a \alpha^2 B_1. \tag{35}$$

The drag coefficient  $D_N$  is determined by the following expression:

$$D_N = \frac{F}{-2\pi\mu_1 U a}. \tag{36}$$

A. Certain limiting cases

**Case I:** If  $l \rightarrow 0$  and  $\alpha \rightarrow 0$ , then the porous sphere of an infinite expanse transforms into a liquid sphere. In this case, the value of drag force is

$$F = \frac{-2a\pi U \mu_1}{3(1 + \lambda^2)} \left[ \frac{32}{63} S^2 + 6\lambda^2 + 9 \right] \text{ with } \lambda^2 = \mu_1 / \mu_2, \tag{37}$$

which was previously reported by Ramkissoon.<sup>30</sup>

**Case II:** If  $S \rightarrow 0$ , then the reduced drag force for all models is given in the [Appendix](#).

**Case III:** If  $\alpha \rightarrow 0$  and  $S \rightarrow 0$ , then the drag force comes out as:

For Happel’s model:

$$F = \frac{4\pi\mu_1 U a \left[ 3 + 2\gamma^{5/3}(-1 + \lambda^2) + 2\lambda^2 \right]}{\left\{ \frac{\gamma^{5/3}(3 - 2\lambda^2) + 2\gamma^2(-1 + \lambda^2)}{+2(1 + \lambda^2) - \gamma^{1/3}(3 + 2\lambda^2)} \right\}}. \tag{38}$$

For Kuwabara’s model:

$$F = - \frac{10\pi\mu_1 U a (3 + 2\lambda^2)}{\left\{ \frac{5\gamma + \gamma^2(-1 + \lambda^2) + 5(1 + \lambda^2)}{-3\gamma^{1/3}(3 + 2\lambda^2)} \right\}}. \tag{39}$$

For Kvashnin’s model:

$$F = \frac{8\pi\mu_1 U a \left[ 3\gamma^{5/3}(-1 + \lambda^2) - 4(3 + 2\lambda^2) \right]}{\left\{ \frac{10\gamma + \gamma^{5/3}(9 - 6\lambda^2) + 8\gamma^2(-1 + \lambda^2)}{+16(1 + \lambda^2) - 9\gamma^{1/3}(3 + 2\lambda^2)} \right\}}. \tag{40}$$

For Mehta–Morse’s model:

$$F = \frac{8\pi\mu_1 U a \left[ 3 + 2\lambda^2 + 3\gamma^{5/3}(-1 + \lambda^2) \right]}{\left\{ (-1 + \gamma^{1/3})^3 \left[ \frac{4\gamma(-1 + \lambda^2) + 4(1 + \lambda^2)}{+ \gamma^{2/3}(-3 + 6\lambda^2) + \gamma^{1/3}(3 + 6\lambda^2)} \right] \right\}}. \tag{41}$$

These results are already reported by Jaiswal and Gupta.<sup>15</sup>

**Case IV:** If  $\lambda^2 \rightarrow 0$ , then the drag force on a rigid sphere reduces as:

For Happel’s model:

$$F = \frac{4\pi\mu_1 U a \left[ 3 + 2\gamma^{5/3} \right]}{2 - 3\gamma^{1/3} + 3\gamma^{5/3} - 2\gamma^2}. \tag{42}$$

This renowned result is available in the classical book.<sup>33</sup>

For Kuwabara’s model:

$$F = \frac{30\pi\mu_1 U a}{-5 + 9\gamma^{1/3} - 5\gamma + \gamma^2}, \tag{43}$$

which is the well-known result reported by Kuwabara.<sup>9</sup>

For Kvashnin’s model:

$$F = \frac{24\pi\mu_1 U a \left[ 4 + \gamma^{5/3} \right]}{-16 + 27\gamma^{1/3} - 10\gamma - 9\gamma^{5/3} + 8\gamma^2}. \tag{44}$$

The above result is earlier proposed by Kvashnin.<sup>10</sup>

For Mehta–Morse’s model:

$$F = \frac{24\pi\mu_1 U a \left[ 1 + \gamma^{1/3} + \gamma^{2/3} + \gamma + \gamma^{4/3} \right]}{\left( -1 + \gamma^{1/3} \right)^3 \left( 4 + 7\gamma^{1/3} + 4\gamma^{2/3} \right)}. \tag{45}$$

The well-known result agrees with the result reported earlier by Mehta–Morse.<sup>11</sup>

**Case V:** If  $\gamma \rightarrow 0$ , the drag on a rigid sphere of radius “ $a$ ” in an infinite expanse of fluid is given as

$$F = -6\pi\mu_1 U a, \tag{46}$$

which was already reported by Stokes.<sup>34</sup>

VII. RESULTS AND DISCUSSION ON DRAG

A. Graphical behavior of drag

The graph of non-dimensional drag coefficient  $D_N$  is sketched vs volume fraction ( $\gamma$ ) in [Fig. 2](#), fluid viscosity ratio parameter ( $\lambda^2$ ) in [Fig. 3](#), and Reiner–Rivlin liquid parameter ( $S$ ) in [Fig. 4](#), respectively. The profiles of tangential velocity in [Fig. 5](#) and normal velocity in [Fig. 6](#), the pressure distribution inside and outer region of the liquid sphere in the [Fig. 7](#), and variation of separation parameter (SEP) with respect to parameter  $\alpha$  for Happel, Kuwabara, Kvashnin, and Mehta–Morse models are given in [Fig. 8](#). A comparison study with the graph of drag coefficient  $D_N$  vs Reiner–Rivlin liquid parameter  $S$  for bounded and unbounded region is given in [Fig. 9](#). Numerical values of SEP for the different values of viscosity parameter  $\lambda^2$  against the permeability parameter  $\alpha$  are shown in [Table I](#).

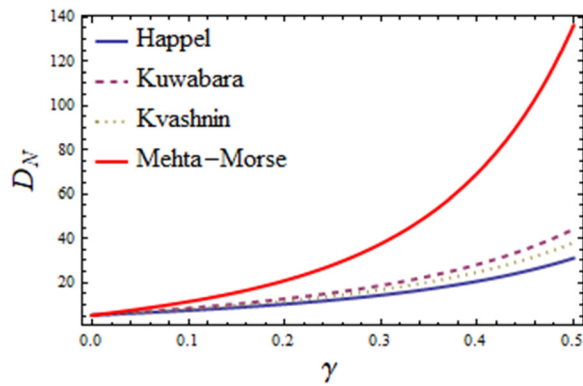


FIG. 2. Plot of drag coefficient  $D_N$  vs volume fraction  $\gamma$  when  $S = 0.5$ ;  $\alpha = 1$ ;  $\lambda^2 = 1$ .

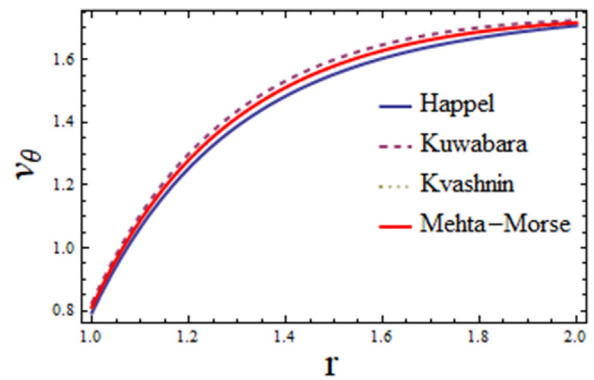


FIG. 5. Plot of tangential velocity vs  $r$  when  $S = 0.5$ ;  $\gamma = 0.05$ ;  $\alpha = 1.5$ ;  $\lambda^2 = 1$ .

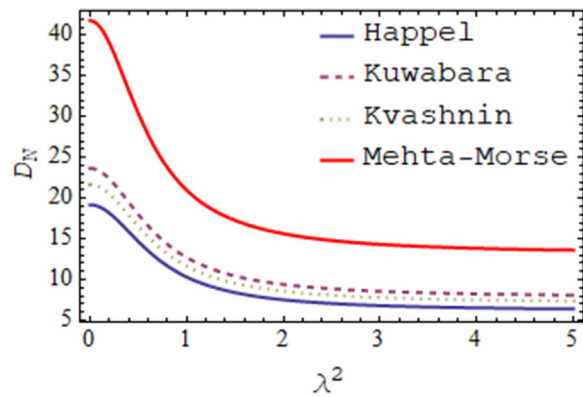


FIG. 3. Plot of drag coefficient  $D_N$  vs viscosity ratio  $\lambda^2$  when  $\alpha = 1$ ;  $\gamma = 0.05$ ;  $S = 0.5$ .

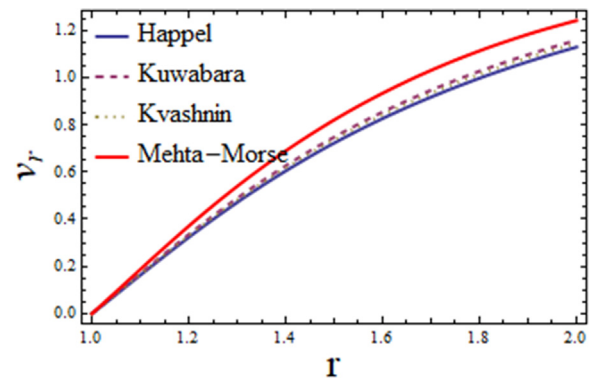


FIG. 6. Plot of normal velocity vs  $r$  when  $S = 0.5$ ;  $\gamma = 0.05$ ;  $\alpha = 1.5$ ;  $\lambda^2 = 1$ .

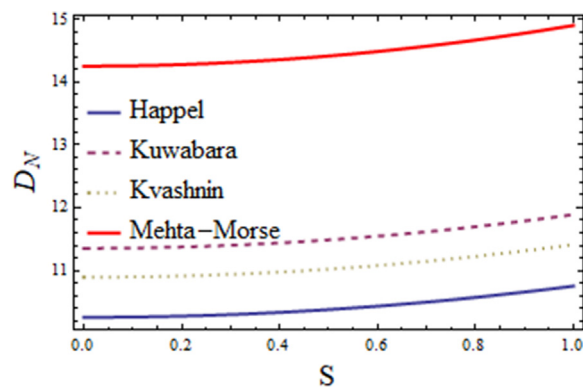


FIG. 4. Plot of drag coefficient  $D_N$  vs cross-viscosity  $S$  when  $\gamma = 0.05$ ;  $\lambda^2 = 1$ ;  $\alpha = 1$ .

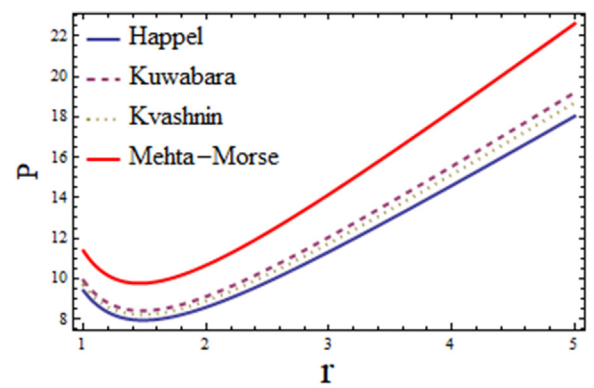


FIG. 7. Plot of pressure vs  $r$  when  $S = 0.5$ ;  $\gamma = 0.05$ ;  $\alpha = 1.5$ ;  $\lambda^2 = 1$ .

The variation of non-dimensional drag coefficient  $D_N$  with respect to the volume fraction  $\gamma$  indicates that the drag coefficient increases monotonically with an increment of the volume fraction  $\gamma$  when other relative parameters remain constant for all four models

(Fig. 2). It is also seen that for  $\gamma < 0.2$  corresponds to a weak drag and increases rapidly for  $\gamma > 0.2$ . Additionally, it can be shown from Fig. 2 that the Mehta-Morse model reports higher drag at high volume fractions. It is interesting to note that a rigid spherical particle's drag is

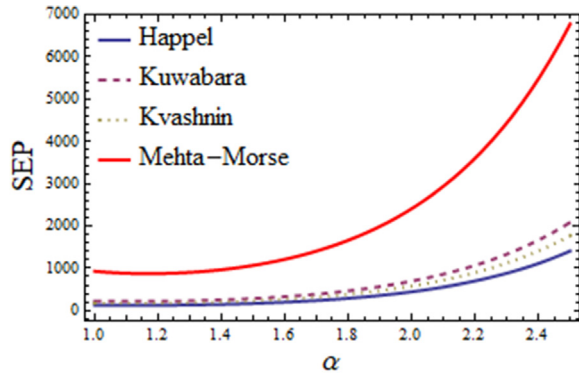


FIG. 8. Plot of separation parameter (SEP) vs permeability parameter  $\alpha$  when  $S = 0.5$ ,  $\gamma = 0.05$ ,  $\lambda^2 = 2$ .

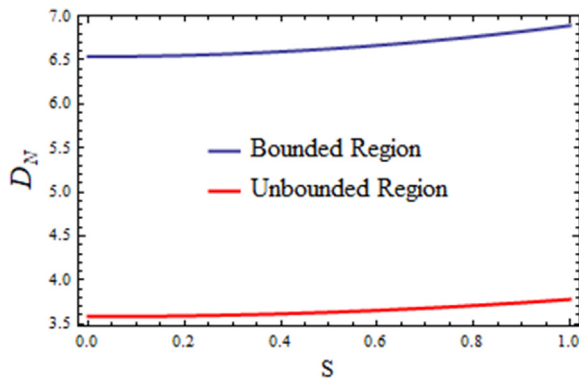


FIG. 9. Plot of drag coefficient  $D_N$  vs  $S$  for bounded and unbounded medium when  $\gamma = 0.05$ ,  $\lambda^2 = 0.2$ ,  $\alpha = 0.9$ .

greater than that of a gaseous spherical bubble in a cell. The Mehta–Morse model deviates from the other three models, as shown in Figs. 2 and 3.

In Fig. 3, the drag coefficient decreases gradually as the viscosity ratio parameter  $\lambda^2$  increases. Here, it is observed that  $\lambda^2 \rightarrow 0$  corresponds to the rigid spherical-in-cell model, and  $\lambda^2 \rightarrow 1$  means that the effective viscosity of the Brinkman medium is the same as that of the clear fluid viscosity. Additionally,  $\lambda^2 \rightarrow \infty$  denotes the gaseous spherical bubble-in-cell model. The graphical representation of non-dimensional drag  $D_N$  with regard to the viscosity ratio  $\lambda^2$  is given in Fig. 3. In each models, we have noticed that the drag rapidly decreases with the variation of viscosity ratio  $\lambda^2$  and further slightly decreases whenever the viscosity ratio increases, and finally remains constant. Fascinatingly, the drag grows gradually for the lowest value of the Happel’s, Kvashnin’s, and Kuwabara’s models, increasing gradually for the greatest feasible value of the Mehta–Morse model.

Figure 4 illustrates the effects of non-dimensional drag coefficient  $D_N$  with respect to the dimensionless parameter  $S$ . It can be observed that the drag  $D_N$  increases slowly with an increase in the liquid sphere. Additionally, it can be observed that the drag decreases gradually with an increase in the classical viscosity ratio  $\lambda^2$ . Physically, it means that the drag  $D_N$  is smaller in the case of the Reiner–Rivlin liquid sphere

TABLE I. Quantitative values of separation parameter for different values of classical viscosity  $\lambda^2$  against the permeability parameter  $\alpha$ .

Cell model	SEP		
	$\lambda^2 = 0.01$	$\lambda^2 = 1$	$\lambda^2 \rightarrow \infty$
Happel model ( $\alpha$ )			
1	68.25	45.11	29.70
1.2	76.48	49.66	32.34
1.4	100.42	63.93	41.14
1.6	147.81	92.17	58.27
1.8	233.89	142.75	89.60
2	385.49	230.24	142.75
Kuwabara model ( $\alpha$ )			
1	75.47	49.10	32.09
1.2	82.98	53.12	34.36
1.4	107.22	67.42	43.12
1.6	155.79	96.12	60.76
1.8	244.01	147.57	92.21
2	398.94	236.41	146.03
Kvashnin model ( $\alpha$ )			
1	72.42	47.44	31.10
1.2	80.22	51.66	33.51
1.4	104.31	65.94	42.28
1.6	152.35	94.42	59.83
1.8	239.61	145.49	91.09
2	393.05	233.72	144.60
Mehta–Morse model ( $\alpha$ )			
1	95.06	59.19	37.87
1.2	101.45	62.36	39.54
1.4	127.54	77.26	48.53
1.6	180.94	107.91	67.12
1.8	277.68	162.89	100.32
2	446.24	257.33	156.92

than that of the rigid sphere. The Mehta–Morse model deviates from Happel, Kuwabara, and Kvashnin models. We concluded from the figure that there is a greater drag at the viscosity ratio  $\lambda^2$  when compared to the other three models.

It can be visualized from the Figs. 5–7 is that there is a very good negotiation among the numerical solutions and analytical results for the normal velocity, tangential velocity, and the pressure distribution. The variation of tangential velocity profile  $v_\theta$  vs radial coordinate  $r$  is given in Fig. 5. The graphs indicate that the tangential velocity increases as the value of radial coordinate  $r$  increases.

The dependence of normal velocity  $v_r$  on  $r$  by keeping values of  $S = 0.5$ ,  $\lambda^2 = 1$ ,  $\gamma = 0.05$ , and  $\alpha = 1.5$  is illustrated in Fig. 6. It is observed that the normal velocity increases with an increasing radius vector  $r$ . It is noted that the normal velocity is slightly lower for all the other three models when compared to the Mehta–Morse model.

The pressure distribution outside the body embedded in a fluid-saturated permeable medium plotted in Fig. 7 for distinct values of  $r$ , also keeping  $\lambda^2 = 1$ ,  $S = 0.5$ ,  $\alpha = 1.5$ , and  $\gamma = 0.05$ , is unchanged.

The effect of pressure distribution begins to decrease along the radius of a vector when it arrives at the minimum value for some definite values of distance ( $r$ ). It is linearly increases beyond this value. However, it is observed that the pressure distribution is slightly lower for all the other three models when compared to the Mehta–Morse model.

The flow separation at rear stagnation point to the sphere is analyzed using the separation parameter (SEP), which is defined by

$$SEP = B_1 + 1 + C_1 \left\{ 1 + \frac{\alpha^2}{2} \right\} K_{\frac{3}{2}}(\alpha) + D_1 \left\{ 1 + \frac{\alpha^2}{2} \right\} I_{\frac{3}{2}}(\alpha). \quad (47)$$

In Fig. 8, it is fascinating to observe that the effect of separation parameter for different values of the parameter  $\alpha$  with fixed values of  $S = 0.5$  and volume fraction  $\gamma = 0.05$ . The variation of SEP with numerical values of viscosity ratio is specified in Table I. Based on the Brinkman model, the flow will not happen at any SEP for the fluid flow on the surface of the liquid sphere. Furthermore, we have seen in the case of smaller values of the classical viscosity ratio increases as increases in the larger value of the separation parameter for all four models. There is excellent agreement, which can be seen in Table I and Fig. 8.

The corresponding variation is shown in Fig. 9, which is comparative study on the drag coefficient exerted by a bounded region and an unbounded region. Finally, it can be concluded from Fig. 9 that the drag is greater in the case of a bounded region than in the case of an unbounded region.

### VIII. GRAPHICAL BEHAVIOR OF STREAMLINES

Streamlines are plotted on the basis of the Happel model, the Kuwabara model, the Kvashnin model, and the Mehta–Morse model. In each case, parameter  $l$  connecting to particle volume fraction  $\gamma$  is chosen as the half of the unity for graphical behaviors of the flow pattern.

#### A. Graphical representation of streamlines with permeability parameter $\alpha$

Streamlines are plotted for permeability parameter ( $\alpha = 0.4$ ) on the basis of the Happel model, the Kuwabara model, the Kvashnin model, and the Mehta–Morse model, and the flow behavior is given in Fig. 10. It can be seen that the flow pattern in the Kuwabara and Kvashnin models is identical, whereas the Mehta–Morse model has a comparable depiction. Streamlines in the Happel model vary greatly depending on the permeability parameter. Streamlines in the Happel model are of a circulatory character at the top and bottom of the inner sphere, pointing in the direction of fluid flow, whereas parabolic insights are visible in the presence of other models.

#### B. Graphical representation of the streamlines with Reiner–Rivlin liquid parameter $S$

Figure 11 illustrates that the behavior of the streamlines in the Happel and Kuwabara models is identical. Fluid layers are pressing against one other on the top and bottom of the sphere in the direction of flow. Some layers in the Kvashnin model are circulatory inside the inner sphere, whereas streamlines push to other layers outside the inner sphere. The streamlines in the Mehta–Morse model follow the circulatory depiction.

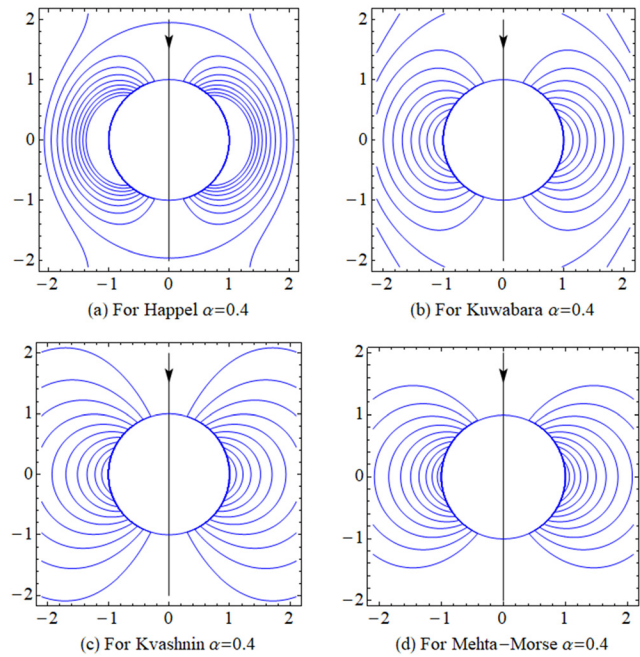


FIG. 10. Graph of streamlines for  $\alpha$  using  $\lambda^2 = 0.5$ ;  $S = 0.3$ ;  $l = 1.2$ ; (a) Happel model, (b) Kuwabara model, (c) Kvashnin model, (d) Mehta–Morse model.

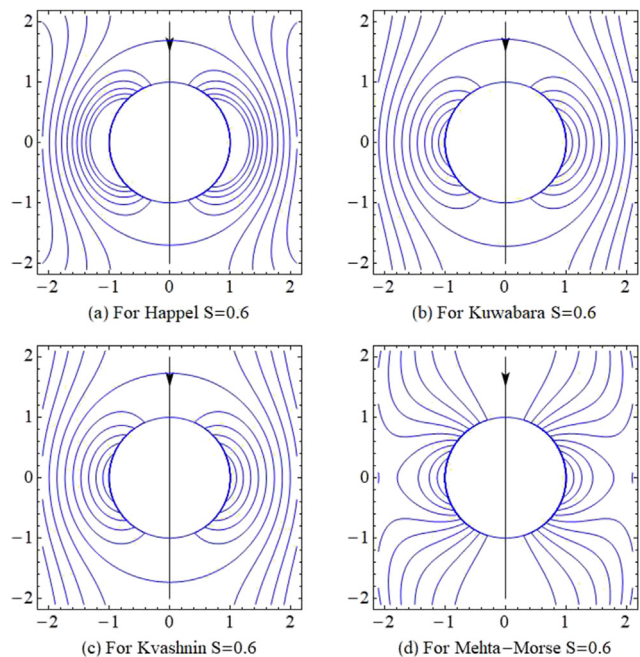
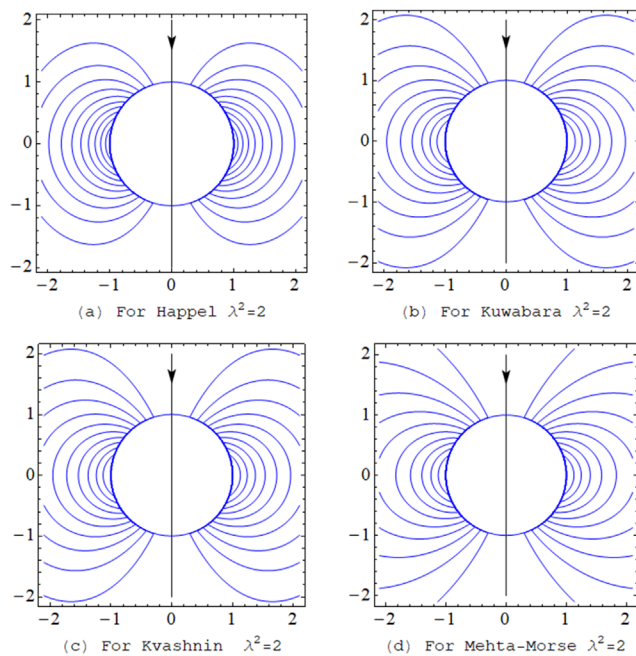


FIG. 11. Graph of streamlines for  $S$  using  $\lambda^2 = 1$ ;  $l = 1.2$ ;  $\alpha = 0.6$ ; (a) Happel model, (b) Kuwabara model, (c) Kvashnin model, (d) Mehta–Morse model.



**FIG. 12.** Graph of streamlines for  $\lambda^2$  using  $S = 0.7$ ;  $l = 1.2$ ;  $\alpha = 0.2$ ; (a) Happel model, (b) Kuwabara model, (c) Kvashnin model, (d) Mehta–Morse model.

### C. Graphical representation of the streamlines with viscosity ratio $\lambda^2$

To compare the flow pattern on the basis of four cell models, streamlines are sketched for fluid viscosity ratio  $\lambda^2 = 2$  with the help of Reiner–Rivlin liquid parameter ( $S = 0.7$ ), permeability parameter  $\alpha = 0.2$ , and thickness of porous layer  $\delta = 0.6$  and the representation of flow behavior is given in Fig. 12. In the change of the viscosity ratio parameter, the flow pattern is identical in the Kuwabara and Kvashnin models. Streamlines in the Happel model and the Mehta–Morse model behave quite differently when the viscosity ratio parameter is increased. Circulatory character can be detected in the inner sphere of the Mehta–Morse model, as well as semi-circulatory appears in the annulus region.

### IX. OUTCOME OF THE WORK

Motivated by applications in non-Newtonian chemical engineering processes involving emulsion droplet motion in porous media, a mathematical model has been developed for steady-axisymmetric creeping Stokesian flow past a Reiner–Rivlin liquid sphere enclosed by a hypothetical spherical porous cell. The motivation of this work is to obtain an analytical solution for the given problem of a Reiner–Rivlin liquid sphere enclosed by a hypothetical spherical porous cell. The situation with the four cell models, namely, Happel, Kuwabara, Kvashnin, and Mehta–Morse conditions, is considered. An expression for the drag force, separation parameter, pressure, and velocity components acting on the liquid sphere is obtained in closed form in terms of the four models, permeability parameter  $\alpha$ , cross-viscosity  $S$ , viscosity ratio  $\lambda^2$ , and the volume fraction  $\gamma$ . The problem was solved analytically as well as numerically using the cell models. The variation of drag coefficient  $D_N$ , separation parameter (SEP), pressure, and velocity profiles is

presented in the graphical form with respect to various parameters. Extensive visualization is included additionally for streamline contours. The following observations are made:

- The non-dimensional drag is the decreasing function of the classical viscosity and increases the function of the volume fraction.
- It has been observed that hydrodynamic permeability is highly dependent on the porosity of the membrane, both apparent and intrinsic, as well as the scale characteristics of the porous layer included in the cell.
- It is found that the drag coefficient on the solid sphere is more than the drag exerted by a non-Newtonian liquid sphere.
- It is observed that the separation parameter is larger than the skin friction on the cell surface.
- An interesting observation is that the variation of drag coefficient, separation parameter, pressure, and the velocity profile is slightly more significant for Mehta–Morse when compared to the Happel, Kuwabara, and Kvashnin models.
- It is interesting to note that the flow patterns are axisymmetric in the initial. After that, it shows that circulatory rotational motion increases the viscosity ratio.
- The patterns of streamlines are also similar to all models except the Mehta–Morse model.
- It is observed from the streamlines that the flow patterns are very pronounced in the boundary as the dimensionless parameter  $S$  increases. Finally, the flow patterns move to circulatory motion at the minimum values of  $S = 0.6$ .

However, this work is more important to the study of the flow of porous fluids through porous rocks of spherical shape, sand beds, earthen soil, petroleum reservoir rocks, in migration of porous media, etc. The valuable contribution and application to industrial, environmental engineering and science, and biomedical are the result of this model. It gives an insight into facts to be taken into account while processing filtration involving polymeric fluids with additives (dopants) and many other such fluids showing similarity with Reiner–Rivlin fluids. The numerous applications of Reiner–Rivlin nanofluids, which facilitate multiple industrial heat transfer processes, have attracted more scientific attention in recent years. These nanofluids are additionally utilized in the pharmaceutical field; some of them contain nanodrugs. Hard drives, understanding turbine systems, jet engines, optical sensors, heating and cooling components, and hard drives are among the items, which utilize these individuals.

### ACKNOWLEDGMENTS

Deepak Kumar Maurya acknowledges the Council of Science and Technology, Uttar Pradesh, India, for the Research Project (Ref. No. CST/D-1517) to carry this research work. The authors extend their gratitude to the referees for their helpful suggestions, which helped to improve the presentation of the manuscript. The authors are also thankful to The Institute of Mathematical Sciences, Chennai, for supporting this work.

### AUTHOR DECLARATIONS

#### Conflict of Interest

The authors have no conflicts to disclose.

**Author Contributions**

**R. Selvi:** Conceptualization (equal); Methodology (equal); Validation (equal); Writing – original draft (equal). **Deepak Kumar Maurya:** Conceptualization (equal); Investigation (equal); Supervision (equal); Validation (equal); Writing – original draft (equal); Writing – review & editing (equal). **Pankaj Shukla:** Formal analysis (equal); Project administration (equal); Supervision (equal); Writing – review & editing (equal). **Ali J. Chamkha:** Project administration (equal); Resources (lead); Supervision (supporting); Validation (lead).

**DATA AVAILABILITY**

The data that support the findings of this study are available from the corresponding author upon reasonable request.

**APPENDIX: DRAG FORCE WHEN REINER-RIVLIN PARAMETER (S) IS ABSENT**

**For Happel’s model:**

$$F = \left[ -9\alpha^3\chi - 3\alpha^5\chi + 27\alpha^3\gamma^{1/3}\chi - 54\alpha\gamma^{2/3}\chi - 18\alpha^3\gamma^{2/3}\chi + 54\alpha\gamma\chi - 6\alpha^3\lambda^2\chi - 3\alpha^5\lambda^2\chi + 18\alpha^3\gamma^{1/3}\lambda^2\chi + 3\alpha^5\gamma^{1/3}\lambda^2\chi - 36\alpha\gamma^{2/3}\lambda^2\chi - 18\alpha^3\gamma^{2/3}\lambda^2\chi + 36\alpha\gamma\lambda^2\chi + 6\alpha^3\gamma\lambda^2\chi + 9\alpha^4\gamma^{1/3}\xi - 27\alpha^2\gamma^{1/3}\xi - 9\alpha^4\gamma^{1/3}\xi + 54\alpha^2\gamma^{2/3}\xi - 54\gamma\xi - 18\alpha^2\gamma\xi + 6\alpha^4\lambda^2\xi + \alpha^6\lambda^2\xi - 18\alpha^2\gamma^{1/3}\lambda^2\xi - 9\alpha^4\gamma^{1/3}\lambda^2\xi + 36\alpha^2\gamma^{2/3}\lambda^2\xi + 6\alpha^4\gamma^{2/3}\lambda^2\xi - 36\gamma\lambda^2\xi - 18\alpha^2\gamma\lambda^2\xi \right] / \left[ -36\alpha\gamma - 24\alpha\gamma\lambda^2 + 3\alpha^3\chi + 18\alpha\gamma^{2/3}\chi - 9\alpha\gamma\chi - 3\alpha^3\gamma\chi + 27\alpha\gamma^{4/3}\chi + 3\alpha^3\lambda^2\chi - 3\alpha^3\gamma^{1/3}\lambda^2\chi + 18\alpha\gamma^{2/3}\lambda^2\chi - 12\alpha\gamma\lambda^2\chi - 3\alpha^3\gamma\lambda^2\chi + 18\alpha\gamma^{4/3}\lambda^2\chi + 3\alpha^3\gamma^{4/3}\lambda^2\chi + 9\alpha^2\gamma^{1/3}\xi + 18\gamma\xi + 9\alpha^2\gamma\xi - 27\gamma^{4/3}\xi - 9\alpha^2\gamma^{4/3}\xi - \alpha^4\lambda^2\xi + 9\alpha^2\gamma^{1/3}\xi - 6\alpha^2\gamma^{2/3}\lambda^2\xi + 18\gamma\lambda^2\xi + 6\alpha^2\gamma\lambda^2\xi + \alpha^4\gamma\lambda^2\xi - 18\gamma^{4/3}\lambda^2\xi - 9\alpha^2\gamma^{4/3}\lambda^2\xi \right].$$

**For Kuwabara’s model:**

$$F = \left[ \alpha \left( -567 - 32S^2 + \frac{567}{\gamma^{1/3}} + \frac{32S^2}{\gamma^{1/3}} + \frac{189\alpha^2}{\gamma^{1/3}} - 378\lambda^2 - 63\alpha^2\lambda^2 + \frac{378\lambda^2}{\gamma^{1/3}} + \frac{189\lambda^2\alpha^2}{\gamma^{1/3}} \right) \chi + \left( 567 + 32S^2 + 189\alpha^2 - \frac{567\alpha^2}{\gamma^{1/3}} - \frac{32S^2\alpha^2}{\gamma^{1/3}} + 378\lambda^2 + 189\alpha^2\lambda^2 - \frac{378\alpha^2\lambda^2}{\gamma^{1/3}} - \frac{63\alpha^4\lambda^2}{\gamma^{1/3}} \right) \xi \right] / \left[ 63\gamma \left( -1/\gamma^{4/3}\alpha(-1 + \gamma^{1/3})(-3\alpha^2 - 3\alpha^2\gamma^{1/3} - 3\alpha^2\gamma^{2/3} + 9\gamma - 3\alpha^2\lambda^2 - 2\alpha^2\gamma^{1/3}\lambda^2 - 2\alpha^2\gamma^{2/3}\lambda^2 + 6\gamma\lambda^2 + \alpha^2\gamma\lambda^2) \chi + \left( 9 + 3\alpha^2 - \frac{3\alpha^2}{\gamma} - \frac{9\alpha^2}{\gamma^{1/3}} + 6\lambda^2 + 3\alpha^2\lambda^2 + \frac{\alpha^4\lambda^2}{\gamma^{4/3}} - \frac{3\alpha^2\lambda^2}{\gamma} - \frac{6\alpha^2\lambda^2}{\gamma^{1/3}} \right) \xi \right].$$

**For Kvashnin’s model:**

$$F = \left[ -32S^2\alpha^2\gamma - 567\alpha^3\chi - 32S^2\alpha^3\chi - 189\alpha^5\chi + 1134\alpha^3\gamma^{1/3}\chi + 64S^2\alpha^3\gamma^{1/3}\chi - 1701\alpha\gamma^{2/3}\chi - 96S^2\alpha\gamma^{2/3}\chi - 567\alpha^3\gamma^{2/3}\chi + 1701\alpha\gamma\chi + 96S^2\alpha\gamma\chi - 378\alpha^3\lambda^2\chi - 189\alpha^5\lambda^2\chi + 756\alpha^3\gamma^{1/3}\lambda^2\chi + 126\alpha^5\gamma^{1/3}\lambda^2\chi - 1134\alpha\gamma^{2/3}\lambda^2\chi - 567\alpha^3\gamma^{2/3}\lambda^2\chi + 1134\alpha\gamma\lambda^2\chi + 189\alpha^3\gamma\lambda^2\chi + 567\alpha^4\xi + 32S^2\alpha^4\xi - 1134\alpha^2\gamma^{1/3}\xi - 64S^2\gamma^{1/3}\xi - 378\alpha^4\gamma^{1/3}\xi + 1701\alpha^2\gamma^{2/3}\xi + 96S^2\alpha^2\gamma^{2/3}\xi - 1701\gamma\xi - 96S^2\gamma\xi - 567\alpha^2\gamma\xi + 378\alpha^4\lambda^2\xi + 63\alpha^6\lambda^2\xi - 756\alpha^2\gamma^{1/2}\lambda^2\xi - 378\alpha^4\gamma^{1/3}\xi + 1134\alpha^2\gamma^{2/3}\lambda^2\xi + 189\alpha^4\gamma^{2/3}\lambda^2\xi - 1134\gamma\lambda^2\xi - 567\alpha^2\gamma\lambda^2\xi \right] / \left[ 63\alpha^2(-18\alpha\gamma - 12\alpha\gamma\lambda^2 + 3\alpha^3\chi + 9\alpha\gamma^{2/3}\chi - 9\alpha\gamma\chi - 3\alpha^3\gamma\chi + 18\alpha\gamma^{4/3}\chi + 3\alpha^3\lambda^2\chi - 2\alpha^3\gamma^{1/3}\lambda^2\chi + 9\alpha\gamma^{2/3}\lambda^2\chi - 9\alpha\gamma\lambda^2\chi - 3\alpha^3\gamma\lambda^2\chi + 12\alpha\gamma^{4/3}\lambda^2\chi + 2\alpha^3\gamma^{4/3}\lambda^2\chi + 6\alpha^2\gamma^{1/3}\xi + 9\alpha\xi + 9\alpha^2\gamma\xi - 18\gamma^{4/3}\xi - 6\alpha^2\gamma^{4/3}\xi - \alpha^4\lambda^2\xi + 6\alpha^2\gamma^{1/3}\lambda^2\xi - 3\alpha^2\gamma^{2/3}\lambda^2\xi + 9\gamma\lambda^2\xi + 6\alpha^2\gamma\lambda^2\xi + \alpha^4\gamma\lambda^2\xi - 12\gamma^{4/3}\lambda^2\xi - 6\alpha^2\gamma^{4/3}\lambda^2\xi) \right].$$

## For Mehta–Morse’s model:

$$F = \left[ 9\alpha^3\chi - 27\alpha\gamma^{1/3}\chi - 9\alpha^3\gamma^{1/3} - 9\alpha^3\gamma^{1/3}\chi + 27\alpha\gamma^{2/3}\chi + 6\alpha^3\lambda^2\chi + \alpha^5\lambda^2\chi - 18\alpha\gamma^{2/3}\lambda^2\chi - 9\alpha^3\gamma^{1/3}\lambda^2\chi + 18\alpha\gamma^{2/3}\lambda^2\chi + 3\alpha^3\gamma^{2/3}\lambda^2\chi - 9\alpha^2\xi - 3\alpha^4\xi + 27\alpha^2\gamma^{1/3}\xi - 27\gamma^{2/3}\xi - 9\alpha^2\gamma^{2/3}\xi - 6\alpha^2\lambda^2\xi - 3\alpha^4\lambda^2\xi + 18\alpha^2\gamma^{1/3}\lambda^2\xi + 3\alpha^4\gamma^{1/3}\lambda^2\xi - 18\gamma^{2/3}\lambda^2\xi - 9\alpha^2\gamma^{2/3}\lambda^2\xi \right] / \left[ \alpha^2(-18\alpha\gamma^{2/3} - 12\alpha\gamma^{2/3}\lambda^2 + 9\alpha\gamma^{1/3}\chi + 9\alpha\gamma\chi - \alpha^3\lambda^2\chi + 9\alpha\gamma^{2/3}\lambda^2\chi - 3\alpha\gamma^{2/3}\lambda^2\chi + 6\alpha\gamma\lambda^2\chi + \alpha^3\gamma\lambda^2\chi + 3\alpha^2\xi + 9\gamma/3\xi - 9\gamma\xi - 3\alpha^2\gamma\xi + 3\alpha^2\lambda^2\xi - 3\alpha^2\gamma^{1/3}\lambda^2\xi + 9\gamma^{2/3}\lambda^2\xi - 6\gamma\lambda^2\xi - 3\alpha^2\gamma\lambda^2\xi) \right],$$

where  $\xi = \sinh\left(\alpha - \frac{\alpha}{\gamma^{1/3}}\right)$  and  $\chi = \cosh\left(\alpha - \frac{\alpha}{\gamma^{1/3}}\right)$ .

## REFERENCES

- <sup>1</sup>D. A. Nield and A. Bejan, *Convection in Porous Media* (Springer, 2006).
- <sup>2</sup>H. C. Brinkman, “A calculation of viscous force exerted by a flowing fluid on dense swarm of particles,” *Appl. Sci. Res.* **1**, 27–34 (1947).
- <sup>3</sup>S. Deo and D. K. Maurya, “Generalized stream function solution of the Brinkman equation in the cylindrical polar coordinates,” *Spec. Top. Rev. Porous Media* **10**(5), 421–428 (2019).
- <sup>4</sup>D. K. Maurya and S. Deo, “Stream function solution of the Brinkman equation in parabolic cylindrical coordinates,” *Int. J. Appl. Comput. Math.* **6**(6), 167 (2020).
- <sup>5</sup>Z. U. A. Warsi, *Fluid Dynamics* (CRC Press, 2006).
- <sup>6</sup>D. Y. Khanukaeva and A. R. Troshkin, “Steady nanocapillary flow: Micropolar approach vs classical models,” *Phys. Fluids* **35**(7), 072005 (2023).
- <sup>7</sup>K. K. Zholkovskij, J. H. Malisyyah, V. N. Shilov, and S. Bhattacharjee, “Electrokinetic phenomena in concentrated disperse systems: General problem formulation and spherical cell approach,” *Adv. Colloid Int. Sci.* **279**, 134–135 (2007).
- <sup>8</sup>J. Happel, “Viscous flow relative to arrays of cylinders,” *AIChE* **5**, 174–177 (1959).
- <sup>9</sup>S. Kuwabara, “The forces experienced by randomly distributed parallel circular cylinder or spheres in a viscous flow at small Reynolds number,” *J. Phys. Soc. Jpn.* **14**, 527–532 (1959).
- <sup>10</sup>A. G. Kvashnin, “Cell model of suspension of spherical particles,” *Fluid Dyn.* **14**, 598–602 (1980).
- <sup>11</sup>G. D. Mehta and T. F. Morse, “Flow through charged membranes,” *J. Chem. Phys.* **63**, 1878–1889 (1975).
- <sup>12</sup>G. M. Moatimid, M. A. A. Mohamed, and K. Elagamy, “Heat and mass flux through a Reiner–Rivlin nanofluid flow past a spinning stretching disc: Cattaneo–Christov model,” *Sci. Rep.* **12**, 14468 (2022).
- <sup>13</sup>S. Deo, A. Filippov, A. Tiwari, S. Vasin, and V. Starov, “Hydrodynamic permeability of aggregates of porous particles with an impermeable core,” *Adv. Colloid Int. Sci.* **164**, 21–37 (2011).
- <sup>14</sup>E. I. Saad, “Stokes flow past an assemblage of axi-symmetric porous spheroidal particles-in-cell models,” *J. Porous Media* **15**, 849–866 (2012).
- <sup>15</sup>B. R. Jaiswal and B. R. Gupta, “Cell models for viscous flow past a swarm of Reiner–Rivlin liquid spherical drops,” *Meccanica* **52**, 69–89 (2016).
- <sup>16</sup>R. Selvi and P. Shukla, “Drag on a fluid sphere embedded in porous medium with zero spin condition,” *Int. J. Pure Appl. Math.* **109**, 171–179 (2016), see <https://acadpubl.eu/jsi/2016-109-si/10/18.pdf>.
- <sup>17</sup>R. Selvi and P. Shukla, “Stokes flow through a porous sphere in a cell surface with zero spin conditions,” *Int. J. Pure Appl. Math.* **120**, 147–155 (2018), see <https://acadpubl.eu/hub/2018-120-8/2/16.pdf>.
- <sup>18</sup>R. Selvi, P. Shukla, and A. K. Singh, “Drag on a Reiner–Rivlin liquid sphere embedded in a porous region placed in a micropolar fluid,” *J. Porous Media* **23**, 613–626 (2020).
- <sup>19</sup>S. Raturi and B. V. R. Kumar, “Effect of insoluble surfactants on the motion of Reiner–Rivlin fluid sphere in a spherical container with Newtonian fluid,” *Z. Angew. Math. Phys.* **72**, 172 (2021).
- <sup>20</sup>B. R. Jaiswal, “Steady Stokes flow of a non-Newtonian Reiner–Rivlin fluid streaming over an approximate liquid spheroid,” *Appl. Comput. Mech.* **14**, 145–162 (2020).
- <sup>21</sup>R. Selvi, P. Shukla, and A. N. Filippov, “Flow around a liquid sphere filled with a non-Newtonian liquid and placed into a porous medium,” *Colloid J.* **82**, 152–203 (2020).
- <sup>22</sup>S. Deo, D. K. Maurya, and A. N. Filippov, “Effect of magnetic field on hydrodynamic permeability of biporous membrane relative to micropolar liquid flow,” *Colloid J.* **83**, 662–675 (2021).
- <sup>23</sup>R. Selvi and P. Shukla, “Analytical solutions of non-Newtonian fluid through a Reiner–Rivlin liquid sphere with cell surface,” *IAENG Int. Appl. Math.* **52**, 811–816 (2022), see [https://www.iaeng.org/IJAM/issues\\_v52/issue\\_4/IJAM\\_52\\_4\\_07.pdf](https://www.iaeng.org/IJAM/issues_v52/issue_4/IJAM_52_4_07.pdf).
- <sup>24</sup>Y. P. Lv, H. Gul, M. Ramzan, J. D. Chung, and M. Bilal, “Bioconvective Reiner–Rivlin nanofluid flow over a rotating disk with Cattaneo–Christov flow heat flux and entropy generation analysis,” *Sci. Rep.* **11**, 15859 (2021).
- <sup>25</sup>R. Selvi, “Drag on a semipermeable spherical particle covered by a couple stress fluid,” *Math. Methods Appl. Sci.* (published online 2023).
- <sup>26</sup>S. Deo and D. K. Maurya, “Investigation of MHD effects on micropolar–Newtonian fluid flow through composite porous channel,” *Microfluid. Nanofluid.* **26**, 64 (2022).
- <sup>27</sup>D. K. Maurya and S. Deo, “Effect of magnetic field on Newtonian fluid sandwiched between non-Newtonian fluids through porous cylindrical shells,” *Spec. Top. Rev. Porous Media* **13**, 75–92 (2022).
- <sup>28</sup>D. K. Maurya, S. Deo, and D. Khanukaeva, “Analysis of Stokes flow of micropolar fluid through a porous cylinder,” *Math. Methods Appl. Sci.* **44**, 6647–6665 (2021).
- <sup>29</sup>S. Deo and S. Kumar, “MHD Reiner–Rivlin liquid flow through a porous cylindrical annulus,” *Appl. Appl. Math.* **16**, 15 (2021), see <https://digitalcommons.pvamu.edu/aam/vol16/iss2/15>.
- <sup>30</sup>H. Ramkissoon, “Stokes flow past a Reiner–Rivlin fluid sphere,” *J. Appl. Math. Mech.* **69**, 259–261 (1989).
- <sup>31</sup>P. K. Maurya, S. Deo, and D. K. Maurya, “Couple stress fluid flow enclosing a solid sphere in a porous medium: Effect of magnetic field,” *Phys. Fluids* **35**, 072006 (2023).
- <sup>32</sup>R. Selvi, D. K. Maurya, and P. Shukla, “Analytical solution of a couple stress fluid saturated in a porous medium through a Reiner–Rivlin liquid sphere,” *Phys. Fluids* **35**, 073106 (2023).
- <sup>33</sup>J. Happel and H. Brenner, *Low Reynolds Number Hydrodynamics* (Martinus Nijhoff Publishers, The Hague, 1983).
- <sup>34</sup>G. G. Stokes, “On the effects of internal friction of fluids on pendulums,” in *Mathematical and Physical Papers* (Cambridge University Press, 2009), pp. 1–10.